Journal of Medicinal Chemistry

Brief Article

pubs.acs.org/jmc

# Inhibitor of Ovarian Cancer Cells Growth by Virtual Screening: A New Thiazole Derivative Targeting Human Thymidylate Synthase

Emanuele Carosati,[†] Anna Tochowicz,[‡] Gaetano Marverti,[§] Giambattista Guaitoli,[∥,#] Paolo Benedetti,[⊥] Stefania Ferrari,[∥] Robert M. Stroud,[‡] Janet Finer-Moore,[‡] Rosaria Luciani,[∥] Davide Farina,[∥] Gabriele Cruciani,*[,†] and M. Paola Costi*[,∥]

[†]Dipartimento di Chimica, Università degli Studi di Perugia, Via Elce di Sotto 10, 06123, Perugia, Italy

[‡]Department of Biochemistry and Biophysics, University of California—San Francisco, 600 16th Street, San Francisco 94158, California, United States

[§]Dipartimento di Scienze Biomediche, Metaboliche e Neuroscienze, Università degli Studi di Modena e Reggio Emilia, Via Campi 287, 41125 Modena, Italy

[∥]Dipartimento di Scienze Farmaceutiche, Università degli Studi di Modena e Reggio Emilia, Via Campi 183, 41125 Modena, Italy

[⊥]Molecular Discovery Limited, 215 Marsh Road, Pinner, Middlesex, London HA5 5NE, U.K.

Supporting Information

**ABSTRACT:** Human thymidylate synthase (hTS) was targeted through a virtual screening approach. The most optimal inhibitor identified, 2-{4-hydroxy-2-[(2-hydroxybenzylidene)hydrazono]-2,5-dihydrothiazol-5-yl}-*N*-(3-trifluoromethylphenyl)-acetamide (**5**), showed a mixed-type inhibition pattern, with a $K_i$ of 1.3 $\mu$M and activity against ovarian cancer cell lines with the same potency as cisplatin. X-ray studies revealed that it binds the inactive enzyme conformation. This study is the first example of a nonpeptidic inhibitor that binds the inactive hTS and exhibits anticancer activity against ovarian cancer cells.

## INTRODUCTION

The only biosynthetic pathway for 2′-deoxythymidine 5′-monophosphate, which is required for DNA synthesis, includes thymidylate synthase (TS), which has been intensively studied as a key anticancer drug target.[1−3] TS is highly conserved;[4] an analysis of 109 TS sequences from pathogenic organisms revealed that more than 75% of these sequences exhibit an overall identity of 40−80% with human TS (hTS). Moreover, 8 of the 32 residues in the active site are invariant in the analyzed TS sequences, and another 14 residues are invariant in more than 80% of these sequences.[5] Most of the ligands that have been cocrystallized with hTS (available in the PDB) and studied as potential anticancer drugs are TS substrates and cofactor analogues that bind to the enzyme active site, where the substrate 2′-deoxyuridine 5′-monophosphate (dUMP) reacts with the cofactor *N*5,*N*10-methylenetetrahydrofolate (mTHF). Among the most extensively evaluated TS inhibitors are 5-fluorodeoxyuridine 5′-monophosphate (FdUMP), the active metabolite of 5-fluorouracil (5-FU, **1**), and the folate analogue raltitrexed (**2**) (Chart 1), which is approved for cancer treatment in Europe.[6]

In addition to raltitrexed, other inhibitors, such as pemetrexed (LY231514),[7] closely resemble the folate cofactor, and the effectiveness of these inhibitors is thus limited by several mechanisms of resistance. Such folate analogues may lead to higher levels of hTS in the cell through competition with hTS mRNA, which purportedly regulates hTS levels by binding to the enzyme or by stabilization of an enzyme conformation that is resistant to proteasomal degradation.[8−10] In one of the most recent attempts to identify compounds to overcome resistance mechanisms, the core features of dUMP and mTHF were abandoned by identifying new chemotypes that are able to bind hTS.[11]

**Chart 1. Structures of 5-FU (1), Raltitrexed (2), cDDP (3), and 4−9 Identified in the SBVS**

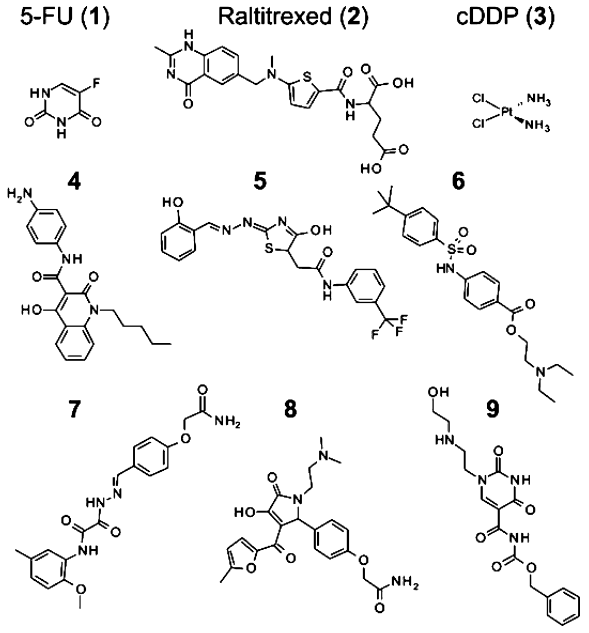


**Received:** June 16, 2012
**Published:** October 17, 2012

Table 1. Human Thymidylate Synthase Enzymatic Activity Inhibition, Cell Growth Inhibition, and Toxicity Data for 4−9[a]

| | | $IC_{50}$ | | | | |
|---|---|---|---|---|---|---|
| compd | hTS $IC_{50}$ or % I | 2008 | C13* | A2780 | A2780/CP | Vero |
| 5-FU (**1**) | *b* | 4.2 ± 0.5 | 8.5 ± 1 | 5.1 ± 0.4 | 12.3 ± 0.8 | 4.5 ± 0.3 |
| cDDP (**3**) | *c* | 1.5 ± 0.1 | 16.2 ± 2 | 2.5 ± 0.4 | 20.3 ± 3.1 | 10.8 ± 1 |
| **4** | 71 ± 5<br>41 ± 3.6[d] | 8.8 ± 2 | 9.2 ± 1.3 | 4.9 ± 1.3 | 12.3 ± 2.1 | 10.2 ± 0.7 |
| **5** | 90 ± 6.3<br>33 ± 3[d] | 21.1 ± 2.5 | 28.3 ± 3 | 19.4 ± 2.5 | 36.4 ± 2.8 | 30.3 ± 3.3 |
| **6** | −<br>15 ± 1.7[e] | >60 | >60 | ND[g] | ND[g] | ND[g] |
| **7** | 112 ± 15<br>35 ± 2.9[f] | >60 | >60 | ND[g] | ND[g] | ND[g] |
| **8** | −<br>16 ± 1.4[e] | 37.4 ± 4.1 | >80 | 16.4 ± 1.3 | 39.5 ± 4.4 | >80 |
| **9** | 619 ± 15<br>36 ± 3.2[e] | 24.1 ± 2.9 | 56.8 ± 4.7 | 6.6 ± 0.7 | 16.5 ± 1.8 | >80 |

[a] $IC_{50}$ values are extrapolated for **4**, **7**, and **9** and was measured for **5**. $IC_{50}$ are reported in μM and is defined as the concentration causing 50% growth inhibition in treated cells when compared to control cells after a 72 h drug exposure. Values represent the mean ± SEM of four separate experiments performed in duplicate. − indicates not soluble for measuring $IC_{50}$. [b] 5-FU is a prodrug. The active inhibitor, FdUMP, exhibits a $K_i$ of 14 nM for hTS. [c] cDDP is not a hTS inhibitor. [d] % inhibition of hTS at 25 μM. [e] % inhibition of hTS at 100 μM. [f] % inhibition of hTS at 50 μM. [g] ND = not determined.

Here, we present the results of a structure-based virtual screening (SBVS) targeting the site to which raltitrexed binds. We have selected and tested 10 non-folate-like new molecules, 6 of which inhibit the hTS enzyme. All of the compounds were tested in ovarian cancer cells that respond to the known drug cisplatin (**3**, cDDP) and the corresponding resistant counterpart cells. Four of the six compounds exhibited inhibitory activities against cDDP-sensitive and -resistant ovarian cancer cells (Table 1, Chart 1). The most potent compound, 2-{4-hydroxy-2-[(2-hydroxybenzylidene)hydrazono]-2,5-dihydrothiazol-5-yl}-*N*-(3-trifluoromethylphenyl)acetamide (**5**), inhibited hTS with a $K_i$ of 1.3 μM and was successfully cocrystallized with hTS, revealing that it binds to the inactive protein conformer.

## RESULTS AND DISCUSSION

**Virtual Screening.** Virtual screening was performed on the SPECS database,[12] which contained approximately 300 000 compounds when it was downloaded from the ZINC archive.[13,14] The use of predicted druglikeness as a filter enhances the possibility of achieving relevant hits and, as in previous successful studies,[11,15] preliminary filtering was performed with the program VolSurf+.[16] For each database compound, a set of physical and biological properties were predicted in silico and used to assess the druglikeness profile of the compound. This calculated profile guaranteed medium-size properties of the drug (MW, volume, and flexibility), a broad lipophilicity range, sufficient solubility, a low rate of metabolism due to CYP 3A4 activity, and low permeability of the blood−brain barrier. After filtering, the database size was significantly reduced from 297 191 structures to 58 837, an elimination of approximately 80% of the compounds. Details of this filtering are provided as Supporting Information.

In the next step, the affinity of each candidate for hTS was estimated with a GRID-based software for virtual screening (FLAP).[17] A receptor-based pharmacophore model was constructed with chain B of the protein 1HVY[18] complexed with dUMP, giving special emphasis to hydrogen bonding interactions occurring with Lys77 and to hydrophobic interactions occurring with Trp109 or Phe225. A fast prefiltering was applied to the large set of 58 837 molecules, and 2852 compounds with the most significant interactions, as evaluated by the "Global Sum" score of FLAP,[19] were retained. Exhaustive calculations were then performed on these molecules, which were ranked again. For this ranking, given the higher precision of the calculations, the distance to the model (FLAP distance score)[19] was used to evaluate the potential inhibitory effect against hTS; the structures and scores are reported as Supporting Information. Compounds **4**−**13** (molecular structures in Chart 1 and the Supporting Information (Tables S1 and S2) were selected among the top 250 ranked compounds, considering also their structural diversity and availability for purchase at the time of the study. These compounds were purchased and tested as described below.

**Human Thymidylate Synthase Inhibition Studies.** Compounds **4**−**13** were evaluated against recombinant hTS, and the percentage inhibition at 25−100 μM was determined. Among these compounds, six exhibited measurable inhibition activity (Table 1). The inhibition ranges of **4**−**9** were between 15% and 41%; **4**, **5**, **7**, and **9** were the most active (Table 1). $IC_{50}$ was estimated between 71 and 619 μM. Detailed study of the inhibition pattern for all compounds was not possible because of their low solubility. The enzyme inhibition pattern of **5** was evaluated in detail against mTHF. At these concentrations, an increase of ∼3.5 times in the $K_m$ and a decrease in $V_{max}$ by 60% were observed. When **5** was evaluated against dUMP, $K_m$ increased of 1.9-fold and $V_{max}$ decreased by ∼80%. The $K_i$ values were 1.3 μM with mTHF as competitor and 2.5 μM with dUMP as competitor. A mixed-type inhibition pattern was observed (Figure S3 in Supporting Information) in both cases.

**X-ray Data Collection and Structure Determination.** The crystal structure of hTS complexed with **5** was obtained. The catalytic loop was in the inactive conformation, with the catalytic Cys195 oriented toward the dimer interface. The eukaryotic insert comprising residues 105−130 was not visible in the density maps. The density corresponding to the insert


dx.doi.org/10.1021/jm300850v | J. Med. Chem. 2012, 55, 10272−10276

comprising residues 143−152 was weak and broken, and residues connecting the two inserts were in a new conformation that impinged on the cofactor binding site (Figure 1a). The

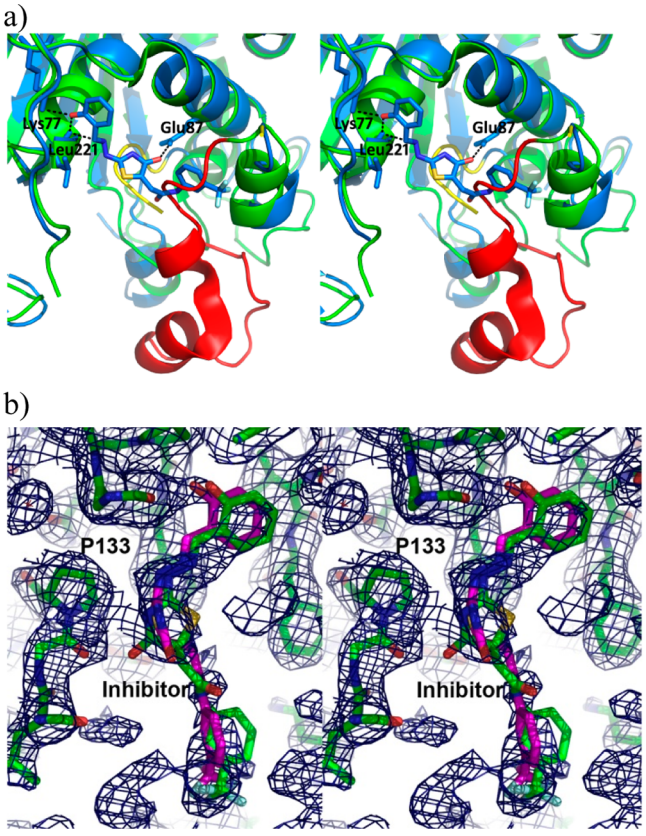


**Figure 1.** (a) Stereo ribbon drawings illustrating two conformations of the variable domain in inactive hTS structures. Apo hTS is shown in green ribbons, with residues 97−134 from the variable domain in red ribbons. Superimposed is the structure of hTS (blue ribbons) cocrystallized with small-molecule inhibitor **5** carbonyl tautomer (shown in blue sticks). In the latter structure, most of the variable domain is disordered, but residues 130−135, shown in yellow ribbons, are oriented in the opposite direction to the corresponding residues in the other structure, implying that the variable domain has a different conformation. The intermolecular hydrogen bonds are shown as broken lines. (b) The $2F_o - F_c$ omit map density ($0.4\sigma$), shown in blue net, was calculated after refining without the ligand. Two partially occupied conformations corresponding to two tautomers of **5** are fit to the density (Supporting Information, Figure S4).

eukaryotic inserts, together with the residues connecting them, are part of a "variable domain" that is present in all TS species. Although the variable domain is not well-conserved among species, this domain contains three conserved residues (Ile108, Trp109, and Asn112 in hTS) that make hydrophobic contacts or hydrogen bonds with the cofactor mTHF in ternary complexes of TS. Thus, the domain has an important role in catalysis but is usually poorly ordered until the cofactor binds. In the new variable domain conformation observed in the cocrystal structure with **5**, the first turn of a conserved two-turn $\alpha$-helix (residues 135−140) is partially unwound, and the N-terminal residue Tyr135 has a left-handed helical conformation. As a result, residues Leu131-Val134 extend from the helix in a direction opposite that of the variable domains in other hTS structures. Although the density for residues 106−130 is not visible, the 9 Å shift in the position of Leu131 implies that these residues must have a different structure than in the apo-enzyme. Inhibitor **5** was built into difference density adjacent to Pro133 in the rearranged loop. The density was well-defined for the phenolic ring, and the linker to the thiazole ring, but was broader for the thiazole ring and weak for the amide linker and trifluoromethyl-substituted phenyl, indicating disorder. We fit the density with two partially occupied conformations with occupancies of 0.68 and 0.32 (Figure 1b). The minor conformation corresponds to the chemical structure shown in Chart 1 (hydroxyl tautomer), while the higher occupancy conformation is likely a tautomer in which the exocyclic double bond to the thiazole has shifted to form a carbonyl instead of the hydroxyl (carbonyl tautomer), allowing the thiazole to rotate out of plane of the phenolic ring (Figures S4 and S5 in Supporting Information). The binding site for the inhibitor overlaps the binding site for the PABA-Glu moiety of mTHF; the phenolic ring is approximately located at the site of polyglutamate binding. The key interactions between the protein side chains and **5** are presented in Figure 1a. The hydroxyl group of the phenolic ring is within hydrogen bonding distance of the Lys77 N−H (2.6 Å) and Leu221 (3.0 Å). Finally, in the minor tautomer, the hydroxyl of the thiazole ring is turned toward the Pro133 carbonyl (2.6 Å) and the Glu87 carboxyl (3.6 Å). Considering the errors in the coordinates of this disordered region of the inhibitor, either or both of these interactions may represent hydrogen bonds. The superposition with the hTS/dUMP/raltitrexed complex (Figure S6 in the Supporting Information) indicates that the major conformational changes are limited mainly to the active site loop (residues 181−197) and hinge (residues 143−152) regions for which density is not visible in the hTS/**5** structure because of the binding mode of **5**.

**Comparison of the X-ray Structures of the Raltitrexed−hTS and 5−hTS Complexes.** The positions of **5** and **2** (raltitrexed) within their binding sites (Figure S6 in Supporting Information) clearly demonstrate a significant overlapping of the hydroxythiazole of **5** with the thiophene of **2** and the phenol of **5** with the terminal acid group of **2**. By contrast, the other molecular extremities differ in their orientations mainly because the presence of dUMP results in a different hydrophobic environment (in the case of 1HVY, see Figure S2 of the Supporting Information). Interestingly, in the case of **5**, no highly favorable interactions involving the phenyl *m*-substituted with trifluoromethyl group were identified. Instead, the relevant hTS-**5** (hydroxyl tautomer) interactions are highlighted in Figure 2, in which the GRID calculation results are illustrated: the hydrophilic interaction of Glu87 with the hydroxyl group at the thiazole ring and the hydrogen bonds of the phenol group with the backbone oxygen of Lys77 and the lateral chain of Leu221.

**Cell Growth Inhibition and Protein Expression Analysis.** The ability of the 10 compounds to inhibit cell growth was evaluated in ovarian cancer cells; the $IC_{50}$ values are reported in Table 1. The dose−response curves for **4**, **5**, **8**, and **9** were compared with those of the known anticancer drugs cDDP and 5-FU, which is the prodrug of FdUMP, a potent TS inhibitor (Figure S8 in the Supporting Information). Compounds **4** and **5** are the most potent of the series, particularly against A2780 and A2780/CP cells, and exhibited the lowest $IC_{50}$ ($IC_{50}$ of 4−13 $\mu$M for **4** and 20−37 $\mu$M for **5**). In addition, the pharmacology of these novel compounds was affected by the resistance phenotype of A2780/CP cells but not that of C13* cells. However, similar to cDDP and 5-FU, these


dx.doi.org/10.1021/jm300850v | J. Med. Chem. 2012, 55, 10272−10276

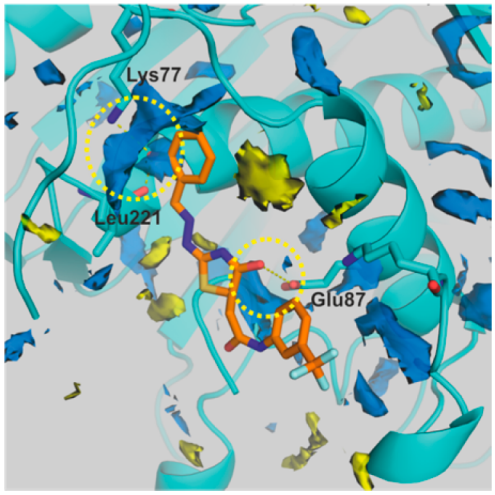


**Figure 2.** Compound **5** is shown within a pocket in hTS, where the GRID hydrophilic MIF (blue, −7.0 kcal/mol) and hydrophobic MIF (yellow, −1.0 kcal/mol) are calculated (in the absence of ligand). The carbon atoms of **5** are shown in orange, whereas the protein is shown in cyan. The phenolic group and the thiazole hydroxyl group are the key molecular features of the ligand−protein interaction and are highlighted by the yellow dot circles.

compounds were not selective and were active and even more potent in Vero cells. Interestingly, although the $IC_{50}$ values of **9** and **8** were higher than those of **4** and **5** in all four ovarian cell lines, **9** and **8** exhibited even better selectivity than cDDP and 5-FU because **9** and **8** were less toxic in Vero cells, with $IC_{50}$ greater than 80 $\mu$M. The data also indicate that the potency of **8** and **9** was affected by the resistance phenotype of C13* and A2780/CP cells (Figure S8 in the Supporting Information). Because **9** represented the best compromise between cytotoxicity against sensitive and resistant cells and selectivity toward the nontumorigenic Vero cell line, the effects of this compound on folate cycle enzyme expression in 2008 and C13* cells were evaluated. As shown in Supporting Information Figure S9, **9** was almost ineffective against TS expression because increasing concentrations of the drug did not significantly decrease TS protein levels in either cell line. In cDDP-sensitive cells, 20 and 40 $\mu$M **9** reduced dihydrofolate reductase (DHFR) protein levels by 40% and 60%, respectively, while resistant cells were unaffected, explaining the observed cross-resistance (2.35-fold).

Because exogenous compounds may oxidize intracellular products, producing hydrogen peroxide and causing cell damage, we investigated ROS production with the fluorescent probe CH-H2DCFDA. In accordance with the resistance phenotype, **9** caused an approximately 1.5- to 2.5-fold increase in reactive oxygen species (ROS) production in 2008 cells but not in C13* cells when compared to the controls (Supporting Information Figure S10). It is likely that the higher content of intracellular detoxifying compounds, such as metallothionein, glutathione, and thioredoxin,[20] allows resistant C13* cells to counteract the toxic effects of **9** better than the sensitive 2008 line.

## CONCLUSIONS

Through a virtual screening approach targeting the raltitrexed folate binding site of hTS, we have identified a thiazole derivative (**5**) that binds the inactive conformer of hTS, in contrast to other known hTS inhibitors. The binding of hTS inhibitors to the inactive conformer was already observed in the case of the recently discovered LR peptide.[21] The X-ray crystal structure of **5**−hTS showed a well-defined density for the phenolic ring, and the linker to the thiazole ring, but broader density for the thiazole ring and weak for the amide linker and trifluoromethyl-substituted phenyl, thus suggesting the existence of two binding tautomers. NMR studies (see Supporting Information, pp S19−S32) only confirmed the structure of **5** in its hydroxyl tautomer (Figure 1), thus suggesting that the protein can stabilize the carbonyl tautomer. In this complex, previously unobserved protein movements and protein−ligand contacts occurred, resulting in different and unexpected binding modes. On the other hand, the computational studies (SBVS and docking) were performed using the hydroxyl tautomer, during the design phase, whose hydroxyl group has HB accepting and donor capabilities. The MIF analysis (Figure 2) revealed the relevance of the HB doning character of the hydroxylthiazole, while X-ray findings suggest no interaction occurring between the carbonyl tautomer and Glu87. This aspect has to be further exploited.

The mixed-type inhibition pattern and the X-ray crystallography data support the allosteric inhibition profile of this compound.

The TS inhibitors identified have been tested in four ovarian cancer cell lines and in Vero cells to gain information on their toxicities. All of the compounds, including **5**, were active against the cancer cells lines; **9** exhibited the most interesting effect against the tumor cells, with no toxicity against Vero cells, and was therefore selected for further biological studies. The effect of **9** on hTS and human DHFR (hDHFR) protein levels in sensitive and resistant ovarian cancer cells suggests that this compound does not affect hTS protein levels but down-regulates hDHFR, as observed for recently discovered peptide inhibitors of hTS.[21] Compound **9** shows higher level of inhibition at the cellular level than against the recombinant hTS; therefore, we reasoned that **9** targets not only hTS but also other proteins such as DHFR. In this work at least two new classes of hTS inhibitors binding the inactive form of the protein have been identified that may show new mechanisms of inhibition against ovarian cancer cells. To further develop the compound classes identified as potential leads for drug development, deeper analysis of the importance of the two tautomers of **5** is necessary, followed by an appropriate medicinal chemistry study to develop compounds with improved efficacy and specificity.

## EXPERIMENTAL SECTION

**Enzyme Inhibition Studies.** All of the tested compounds were purchased with a purity of at least 95%. The *E. coli* strain expressing wild-type recombinant hTS was used as previously reported.[21] After TS purification, the TS activity was spectrophotometrically measured as previously reported.[22]Details are reported in the Supporting Information.

**X-ray Crystallography Data Collection and Structure Determination.** Data collection, processing statistics, *R* factors, and final models are in the Supporting Information (Table S5).

**Cellular Pharmacology.** The molecules were evaluated in five cell lines: human ovarian carcinoma 2008; the cDDP-resistant C13* subline, which is ∼15-fold resistant to cDDP;[23] human ovarian carcinoma A2780; A2780/CP, which is derived from the parent A2780 cell line and is 10-fold resistant to cDDP than the parent cell line; Vero,[24] which was chosen as a control.[25] Cytotoxicity was calculated by comparing cultures exposed to the drug to unexposed (control) cultures. Details are in the Supporting Information.

## ■ ASSOCIATED CONTENT

### Supporting Information

Structures, IUPAC names, and the ZINC and SPECS codes of the tested compounds (Tables S1 and S2); purity of the tested compounds (Table S3); details of the virtual screening (p S7); enzymatic assays (p S10); X-ray experiments (p S12); cellular assays (p S15). This material is available free of charge via the Internet at http://pubs.acs.org.

### Accession Codes

The atomic coordinates for 4E28 have been deposited in the Protein Data Bank.

## ■ AUTHOR INFORMATION


### Corresponding Author

*For G.C.: phone, 0039-075-5855550; fax, 0039-075-45646; e-mail, gabri@chemiome.chm.unipg.it. For M.P.C.: phone, 0039-059-2055134; fax, 0039-059-2055131; e-mail, mariapaola.costi@unimore.it

### Present Address

[#]Medizinisches Proteom Zentrum Nägelestraße 5, 72074 Tübingen, Germany.


### Notes

The authors declare no competing financial interest.

## ■ ACKNOWLEDGMENTS

This work was supported by the LIGHTS project within the 6FP (Grant LSHC-CT-2006-037852; www.lights-eu.org), "Associazione Angela Serra per la Ricerca sul Cancro" to G.M., Modena, Italy, Grant AIRC-DROC IG10474 to M.P.C. We thank Dr. James Holton and Dr. George Meigs for assistance at ALS beamline 8.3.1. Beamline 8.3.1 was funded by the National Science Fundation, University of California—Berkeley, University of California—San Francisco, and Henry Wheeler.

## ■ ABBREVIATIONS USED

cDDP, cisplatin; DHFR, dihydrofolate reductase; dUMP, 2′-deoxyuridine 5′-monophosphate; FdUMP, 5-fluorodeoxyuridine 5′-monophosphate; 5-FU, 5-fluorouracil; hDHFR, human dihydrofolate reductase; hTS, human thymidylate synthase; $IC_{50}$, concentration of inhibitor causing 50% growth inhibition in treated cells; $K_i$, inhibition constant; mTHF, *N*5,*N*10-methylenetetrahydrofolate; TS, thymidylate synthase; MIF, molecular interaction field; PDB, Protein Data Bank

## ■ REFERENCES


(1) Carreras, C. W.; Santi, D. V. The catalytic mechanism and the structure of thymidylate synthase. *Annu. Rev. Biochem.* **1995**, *64*, 721−762.

(2) Stroud, R. M.; Finer-Moore, J. S. Conformational dynamics along an enzymatic reaction pathway: thymidylate synthase, "the movie". *Biochemistry* **2003**, *42*, 239−247.

(3) Finer-Moore, J. S.; Santi, D. V.; Stroud, R. M. Lessons and conclusions from dissecting the mechanism of bisubstrate enzyme: thymidylate synthase mutagenesis, function and structure. *Biochemistry* **2003**, *42*, 248−256.

(4) Perry, K. M.; Fauman, E. B.; Finer-Moore, J. S.; Montfort, W. R.; Maley, G. F.; Maley, F.; Stroud, R. M. Plastic adaptation toward mutations in proteins: structural comparison of thymidylate synthases. *Proteins* **1990**, *8*, 315−333.

(5) Ferrari, S.; Losasso, V.; Costi, M. P. Sequence-based identification of specific drug target regions in the thymidylate synthase enzyme family. *ChemMedChem* **2008**, *3*, 392−401.

(6) Almog, R.; Waddling, C. A.; Maley, F.; Maley, G. F.; Van Roey, P. Crystal structure of a deletion mutant of human thymidylate synthase Delta (7-29) and its ternary complex with Tomudex and dUMP. *Protein Sci.* **2001**, *10*, 988−996.

(7) Shih, C.; Chen, V. J.; Gossett, L. S.; Gates, S. B.; MacKellar, W. C.; Habeck, L. L.; Shackelford, K. A.; Mendelsohn, L. G.; Soose, D. J.; Patel, V. F.; Andis, S. L.; Bewley, J. R.; Rayl, E. A.; Moroson, B. A.; Beardsley, G. P.; Kohler, W.; Ratnam, M.; Schultz, R. M. LY231514, a pyrrolo[2,3-*d*]pyrimidine-based antifolate that inhibits multiple folate-requiring enzymes. *Cancer Res.* **1997**, *57*, 1116−1123.

(8) Chu, E.; Allegra, C. J. The role of thymidylate synthase as an RNA binding protein. *BioEssays* **1996**, *18*, 191−198.

(9) Kitchens, M. E.; Forsthoefel, A. M.; Rafique, Z.; Spencer, H. T.; Berger, F. G. Ligand-mediated induction of thymidylate synthase occurs by enzyme stabilization. *J. Biol. Chem.* **1999**, *274*, 12544−12547.

(10) Sayre, P. H.; Finer-Moore, J. S.; Fritz, T. A.; Biermann, D.; Gates, S. B.; MacKellar, W. C.; Patel, V. F.; Stroud, R. M. Multi-targeted antifolates aimed at avoiding drug resistance form covalent closed inhibitory complexes with human and *Escherichia coli* thymidylate synthases. *J. Mol. Biol.* **2001**, *313*, 813−829.

(11) Carosati, E.; Sforna, G.; Pippi, M.; Marverti, G.; Ligabue, A.; Guerrieri, D.; Piras, S.; Guaitoli, G.; Luciani, R.; Costi, M. P.; Cruciani, G. Ligand-based virtual screening and ADME-Tox guided approach to identify triazolo-quinoxalines as folate cycle inhibitors. *Bioorg. Med. Chem.* **2010**, *18*, 7773−7785.

(12) http://www.specs.net.

(13) http://zinc.docking.org.

(14) Irwin, J. J.; Shoichet, B. K. ZINC—a free database of commercially available compounds for virtual screening. *J. Chem. Inf. Model.* **2005**, *45*, 177−182.

(15) Carosati, E.; Budriesi, R.; Ioan, P.; Ugenti, M. P.; Frosini, M.; Fusi, F.; Corda, G.; Cosimelli, B.; Spinelli, D.; Chiarini, A.; Cruciani, G. Discovery of novel and cardioselective diltiazem-like calcium channel blockers via virtual screening. *J. Med. Chem.* **2008**, *51*, 5552−5565.

(16) http://www.moldiscovery.com/soft_vsplus.php Volsurf+ 1.0.4.

(17) http://www.moldiscovery.com.

(18) Phan, J.; Koli, S.; Minor, W.; Dunlap, R. B.; Berger, S. H.; Lebioda, L. Human thymidylate synthase is in the closed conformation when complexed with dUMP and raltitrexed, an antifolate drug. *Biochemistry* **2001**, *40*, 1897−1902.

(19) Cross, S.; Baroni, M.; Carosati, E.; Benedetti, P.; Clementi, S. FLAP: GRID molecular interaction fields in virtual screening. Validation using the DUD data set. *J. Chem. Inf. Model.* **2010**, *50*, 1442−1450.

(20) Marzano, C.; Gandin, V.; Folda, A.; Scutari, G.; Bindoli, A.; Rigobello, M. P. Inhibition of thioredoxin reductase by auranofin induces apoptosis in cisplatin-resistant human ovarian cancer cells. *Free Radical Biol. Med.* **2007**, *42*, 872−881.

(21) Cardinale, D.; Guaitoli, G.; Tondi, D.; Luciani, R.; Henrich, S.; Salo-Ahen, O. M.; Ferrari, S.; Marverti, G.; Guerrieri, D.; Ligabue, A.; Frassineti, C.; Pozzi, C.; Mangani, S.; Fessas, D.; Guerrini, R.; Ponterini, G.; Wade, R. C.; Costi, M. P. Protein−protein interface-binding peptides inhibit the cancer therapy target human thymidylate synthase. *Proc. Natl. Acad. Sci. U.S.A.* **2011**, *108*, E542−E549.

(22) Liu, Y.; Santi, D. V. A continuous spectrophotometric assay for thymidine and deoxycytidine kinases. *Anal. Biochem.* **1998**, *264*, 259−262.

(23) Andrews, P. A.; Albright, K. D. Mitochondrial defects in cis-diamminedichloroplatinum(II)-resistant human ovarian carcinoma cells. *Cancer Res.* **1992**, *52*, 1895−1901.

(24) Bianchi, N. O.; Ayres, J. Heterochromatin location on chromosomes of normal and transformed cells from African green monkey (*Cercopithecus aethiops*). DNA denaturation−renaturation method. *Exp. Cell Res.* **1971**, *68*, 253−258.

(25) Rossi, T.; Coppi, A.; Bruni, E.; Ruberto, A.; Santa-chiara, S.; Baggio, G. Effects of anti-malarial drugs on MCF-7 and Vero cell replication. *Anticancer Res.* **2007**, *27*, 2555−2559.